

MID-TERM REVIEW RESULTS OF THE ESA STSE PATHFINDER CHARMING PROJECT (CONSTRAINING SEISMIC HAZARD MODELS WITH INSAR AND GPS)

J.P. Merryman Boncori⁽¹⁾, R. Devoti⁽¹⁾, F. Visini⁽²⁾, M.M.C. Carafa⁽³⁾, G. Pezzo⁽¹⁾, G. Fornaro⁽⁴⁾, P. Bernardino⁽⁴⁾, S. Atzori⁽¹⁾, V. D'Amico⁽²⁾, V. Kastelic⁽³⁾, C. Meletti⁽²⁾, G. Pietrantonio⁽¹⁾, F. Riguzzi⁽¹⁾, S. Salvi⁽¹⁾, D. Fernandez Prieto⁽⁵⁾

(1) Istituto Nazionale di Geofisica e Vulcanologia (INGV), Centro Nazionale Terremoti, Via di Vigna Murata 605, 00143 Roma, Italy, john.merryman@ingv.it

(2) INGV, Sezione di Pisa, Via della Faggiola 32, 56126 Pisa, Italy,

(3) INGV, Tettonofisica e Vulcanologia, Via dell'Arcivescovado 8, 67100 L'Aquila, Italy.

(4) Istituto per il Rilevamento Elettromagnetico dell'Ambiente (IREA) del Consiglio Nazionale delle Ricerche (CNR), Via Diocleziano 328, 80124 Napoli, Italy.

(5) ESA/ESRIN, Via Galileo Galilei, 00044 Frascati (Roma), Italy.

ABSTRACT

We probe the feasibility of integrating GPS and Synthetic Aperture Radar deformation rates within the seismic hazard models of the central Apennines (Italy), exploiting data from over 100 GPS stations and the ~20-year long ERS and ENVISAT SAR image archive. We then use a kinematic finite element model to derive the long-term strain rates, as well as earthquake recurrence relations. In turn these are input to state-of-the-art probabilistic seismic hazard models, the output of which is validated statistically using data from the Italian national accelerometric and macroseismic intensity databases.

1. INTRODUCTION

The CHARMING project (Constraining Seismic Hazard Models with InSAR and GPS) is a feasibility study funded by the European Space Agency's (ESA) Support to Science Element (STSE) Pathfinders 2013 programme. The context of CHARMING is Probabilistic Seismic Hazard Assessment (PSHA), i.e. the scientific field which aims to quantify the probability that ground motion at a specified site will exceed some level of a given shaking parameter of engineering interest (e.g. Peak Ground Acceleration, PGA) during a specified future time frame. The main aim of the project is to investigate whether surface deformation measurements, derived from GPS and Synthetic Aperture Radar (SAR) data, can be successfully incorporated into PSHA models and improve their quality. In particular, we investigate several aspects related to the marginal benefit provided by the integration of SAR compared to GPS alone, since to our best knowledge this project represents the first attempt worldwide to incorporate SAR measurements into PSHA models.

2. METHODOLOGY

Our approach is summarized in Fig. 1. Firstly, we generate interseismic velocity maps of our areas of

interest using a combination of permanent GPS stations (Fig. 2) and coast-to-coast acquisitions of the ERS-1/2 AMI and ENVISAT ASAR satellite SAR sensors (Fig. 3). From these, long-term strain rates and earthquake rates are derived (i.e. the number of earthquakes in a given time period above an established magnitude threshold). Finally, state of the art PSHA modelling techniques are used to generate probabilistic models for PGA and other shaking parameters. A statistical validation of the PSHA model output is then carried out, using data from national accelerometric and macroseismic intensity databases.

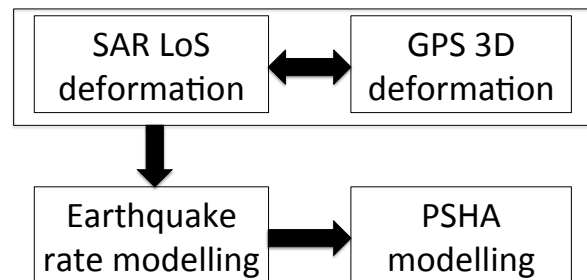


Figure 1. CHARMING workflow

2.1. GPS data processing

GPS data reduction was performed using the Bernese post-processing software ver. 5.0 [1], reprocessing the whole set of available GPS data following the Guidelines for EUREF Analysis Centres (<http://www.epncb.oma.be>). Daily solutions of the whole network of permanent stations were obtained by forming Ionosphere Free linear combinations of GPS observables to account for ionosphere delay and solving for additional parameters, like the troposphere bias and phase ambiguity using the Quasi Ionosphere Free approach. The GPS orbits and the Earth's orientation parameters were fixed to the combined IGS products and an *a priori* loose constraint of 10 m is assigned to all site coordinates. To express the GPS time series in a unique reference frame, the daily solutions were subject

to two main transformations. First the loose covariance matrix was projected imposing tight internal constraints (at millimetre level), and then coordinates were transformed into the ITRF2008 reference frame [2] by a 4-parameter Helmert transformation (translations and scale factor). The regional reference frame transformation uses 45 sites located in central Europe as anchor stations for the reference frame realization. To account for common translations of the entire network, the time series was readjusted through a common mode filtering procedure similar to that proposed by [3]. Velocities at GPS stations were estimated fitting simultaneously a linear drift, episodic offsets and annual sinusoids to the network coordinate time series. Offsets were estimated whenever a change in the GPS equipment induces a significant transient in the time series. Outlier coordinates were rejected whenever the weighted residuals exceed 3.5 times the global chi-square.

To account for the post-seismic deformation of the Mw 6.3 April 6, 2009 L'Aquila earthquake (the only major seismic event within the data spatio-temporal coverage), for all permanent stations within a 50 km radius from its epicentre, we masked out the measurements carried out in a time window of 600 days after the earthquake, and retained only stations with a long-lasting observational history (>6 years) before the event. After this refinement, a total number of 106 permanent were selected.

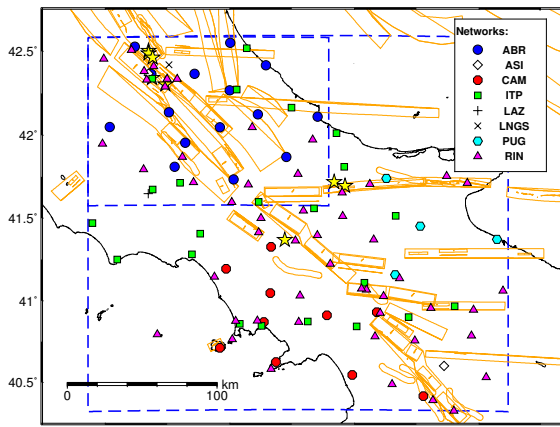


Figure 2. GPS stations and networks within the development (smaller) and experimental (larger) areas (dashed blue rectangles). Orange polygons represent composite and individual seismogenic sources according to the DISS v.3.1.1 catalogue [4]. Yellow stars represent major earthquakes ($M_w > 5.0$), occurred since 1992.

2.2. SAR data processing

SAR line-of-sight (LoS) deformation rate maps were derived with the combined Persistent Scatterer and Small Baseline approach of [5], implemented in the

StaMPS (Stanford Method for Persistent Scatterers) software and with the Intermittent SBAS (ISBAS) approach of [6].

StaMPS was applied to two descending (T036 and T308) and one ascending pass (T129) of the ENVISAT ASAR sensor (Fig. 3). Only imagery acquired prior to Apr. 6, 2009 (the date of the Mw 6.3 L'Aquila earthquake) was used. This yielded data stacks of 27 to 37 images, from which redundant interferogram networks of 145 to 202 interferograms were formed. A quadratic correction was applied to each interferogram to account for the ASAR Local Oscillator drift [7], and no "orbital ramp" estimation was carried out. For all datasets conservative processing parameters (weed standard deviation between 0.7 and 0.8 rad; merge resample size = 0; unwrapping grid = 100 m) were found to improve the accuracy of the results in terms of internal consistency (residual phase misclosures) and agreement with LoS-projected GPS velocities.

ISBAS was applied to a stack of 33 ERS-1/2 and 37 ENVISAT acquisitions from ascending T129, forming a network of 200 interferograms, filtered with a 4×20 multi-looking factor in range and azimuth respectively. Mean velocities were estimated for points with coherence better than 0.15 in at least 130 interferograms.

The resulting mean velocity maps were then calibrated with the LoS-projected GPS measurements for stations with formal uncertainties < 1 mm/yr in all three Cartesian components. Low order polynomial models (degree < 2), with (lat,lon) coordinates as the independent variables, were estimated from the difference between the average of the SAR velocities in a 1 km radius around the GPS station and the GPS velocities themselves. Estimations were carried out separately for a set of manually outlined regions, within which phase unwrapping results appeared to be consistent for most interferograms.

LoS measurements as well as the North velocity component of the GPS were resampled to a common 200 m posting grid. For each grid point for which at least one ascending and one descending measurement were available, a least squares inversion for the East and up velocity components was carried out.

Finally, a median filter was applied using a window with a 2.5 km radius, to average and subsample the East and Up velocity components for subsequent modelling.

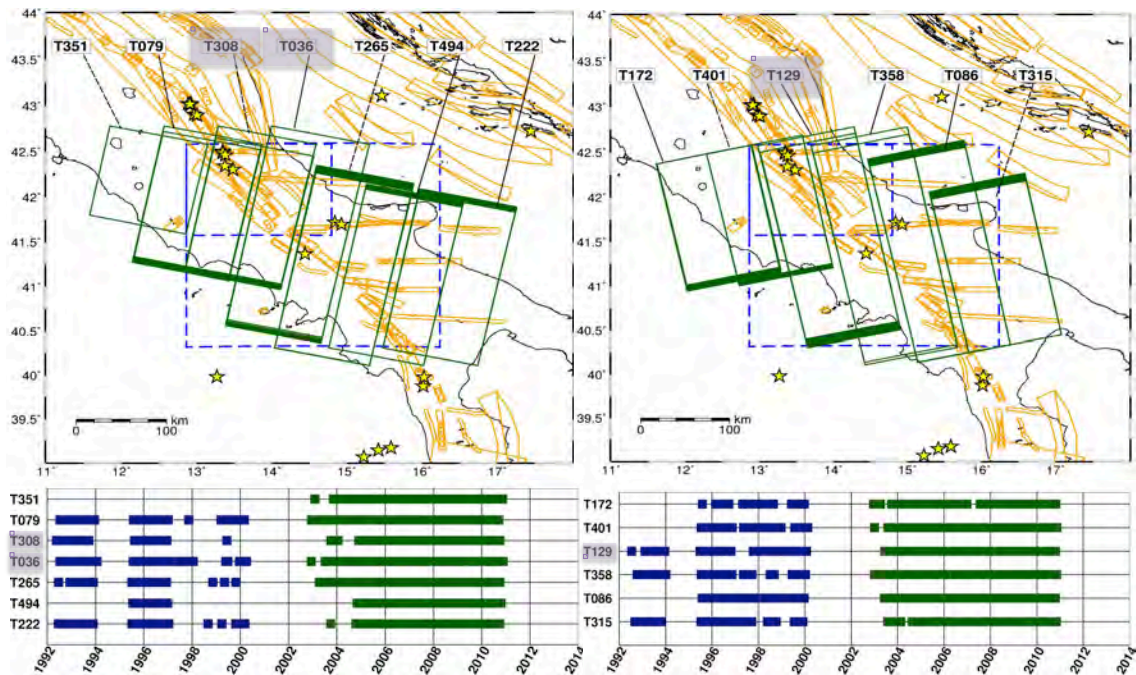


Figure 3. Spatio-temporal coverage of ERS-1/2 (dark blue) and ENVISAT ASAR IS2 (dark green) descending (left) and ascending passes (right). Highlighted tracks were processed at the time of writing. See also caption of Fig. 2.

2.3. Earthquake rate modelling

In a first step, we used the NeoKinema code [8] to model the surface strain rates. The latter uses geodetic measurements as additional constraints in a viscous-shell model of the lithosphere and computes long-term-average horizontal velocities and permanent strain rates for continuum elements. NeoKinema is a kinematic modelling program, which accepts velocity boundary conditions, and fits the internal velocity field within a specified model domain to available geodetic data by a weighted-least-squares method. The domain is represented by a 2-D finite element mesh of spherical triangles in which each node has two degrees-of-freedom, namely the southward and eastward components of long-term-average velocity.

In a second step, the strain rates output by the NeoKinema model are converted to maps of expected seismicity for the area of interest using the program Long_Term_Seismicity_v3, which realizes the two hypotheses of the Seismic Hazard Inferred From Tectonics (SHIFT) model [9]: (a) calculations of the seismic moment rate for any deforming volume should use the coupled seismogenic thickness of the most comparable type of plate boundary and (b) calculations of the earthquake rate should use the seismic moment rate in conjunction with the frequency-magnitude distribution describing the most comparable plate boundary type. The seismicity coefficients (coupled seismogenic lithosphere thickness, corner magnitude

Mc, and asymptotic spectral slope b of the tapered Gutenberg-Richter frequency/moment relationship) were determined by [10] for classes of plate boundaries. An algorithm for assigning the “most comparable” plate boundary can be found in [9], Tables 1, 2.

2.4. Seismic hazard modelling

Seismic hazard assessment (SHA) was carried out following the steps of consolidated approaches [11,12]. The first modeling step is the definition of seismogenic sources, which in this project are represented by points on a 0.1° spaced longitude/latitude grid, with long-term earthquake rates calculated as described in section 2.3. Given a set of earthquake sources with their associated earthquake occurrence characteristics, one or more ground motion predictive models (GMPMs) have then to be used to obtain PSHA models.

Because the test region is subject to various tectonic regimes, we need to associate each point with the appropriate tectonics, in order to assume the most appropriate faulting-style and GMPM parameters. To this aim we identified 7 regions with different faulting styles basing on the distribution and characteristics of known seismogenic sources and focal mechanism solutions. We then used the GMPM developed by [13], derived for the geometrical mean of the horizontal and vertical components, considering the latest available release of the strong motion database for Italy. Finally, we used the OpenQuake hazard engine [14] to compute

annual frequencies of exceedance for a suite of PGA levels (from 0.0001g to 3.4g) on a grid with a 5 km x 5 km posting. We assumed a Poisson earthquake occurrence model for the deforming sources, which results in a time-independent PSHA model.

3. RESULTS

3.1. GPS and SAR deformations

GPS Cartesian velocity components are shown in Fig. 4, whereas SAR LoS and East/Up Cartesian components are shown in Fig. 6 and Fig. 7. Our deformation maps show several signals ascribable to the local tectonics. The GPS vertical component (Fig. 4A) shows an overall NW-SE oriented uplift along the central Apennines from 0.5 to more than 2 mm/yr, which could be attributed to the general NE-SW oriented extension of the Apennines [15]. Some local subsiding stations are also recognized, namely SMRA, CHIE, LPEL and VTRA. For the latter three, the subsidence is likely to be very local. However, that of SMRA, possibly associated to the combined action of sediment compaction and ground water pumping, appears to have a larger spatial scale in the SAR measurements (Fig. 6 and 7), so that a tectonic contribution cannot be entirely excluded.

The GPS east and north velocities (Fig. 4B and 4C) show a regional pattern broadly consistent with the NE-SW Apenninic extension, although at a more local scale several interesting velocity gradients can be observed. Two of these in particular, located at the upper and lower edges of the development area (north of the INGP station and around the ALRA station), are associated with N-S transitions between seismic sources and intense seismic activity, both historically [16] and in the timespan of the geodetic measurements (1992-2008) (Fig. 5).

At the southern edge of the development area, a > 1 mm/yr extension between the SORA-BLRA-VVLO-OTRA and the ALRA-RNI2-CERA blocks is seen. The same area shows shortening velocity gradients in the GPS North component (> 1 mm/yr), resulting in a general NE-SW oriented left-lateral deformation zone located between the Matese mountains to the south, and the Marsica ones to the north.

In the NW part of the development area, the MTER-MTRA block moves westward (~ 1 mm/yr) and southward (~ 2 mm/yr) with respect the MTTO-INGP-AQUI block, which shows eastward and northward movements. These velocities result in a left-lateral deformation zone located north of L'Aquila (AQUI), where some seismic sources give place to others to the north.

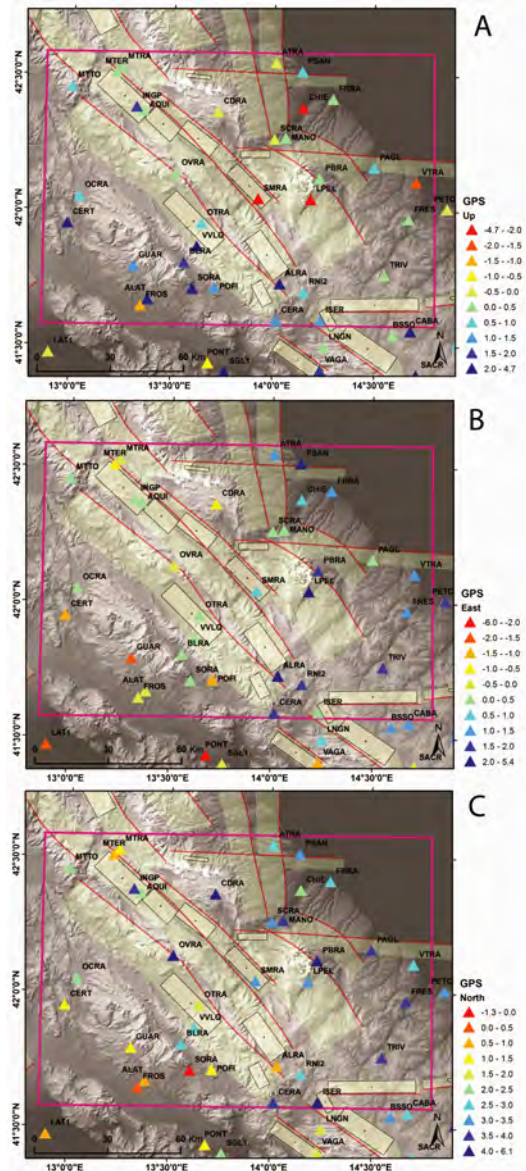


Figure 4. UP (A), East (B) and North (C) GPS velocities, development area (purple rectangle) and DISS catalogue seismic sources.

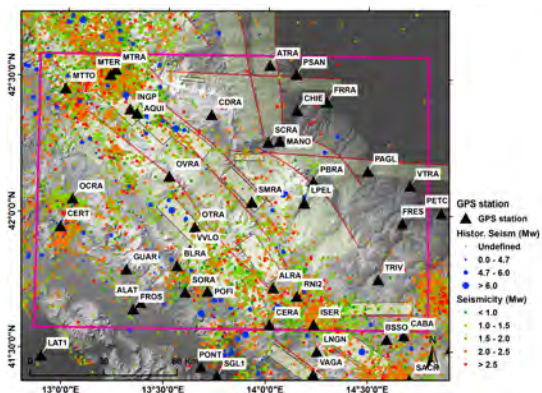


Figure 5. Historical and instrumental seismicity (1992-2008).

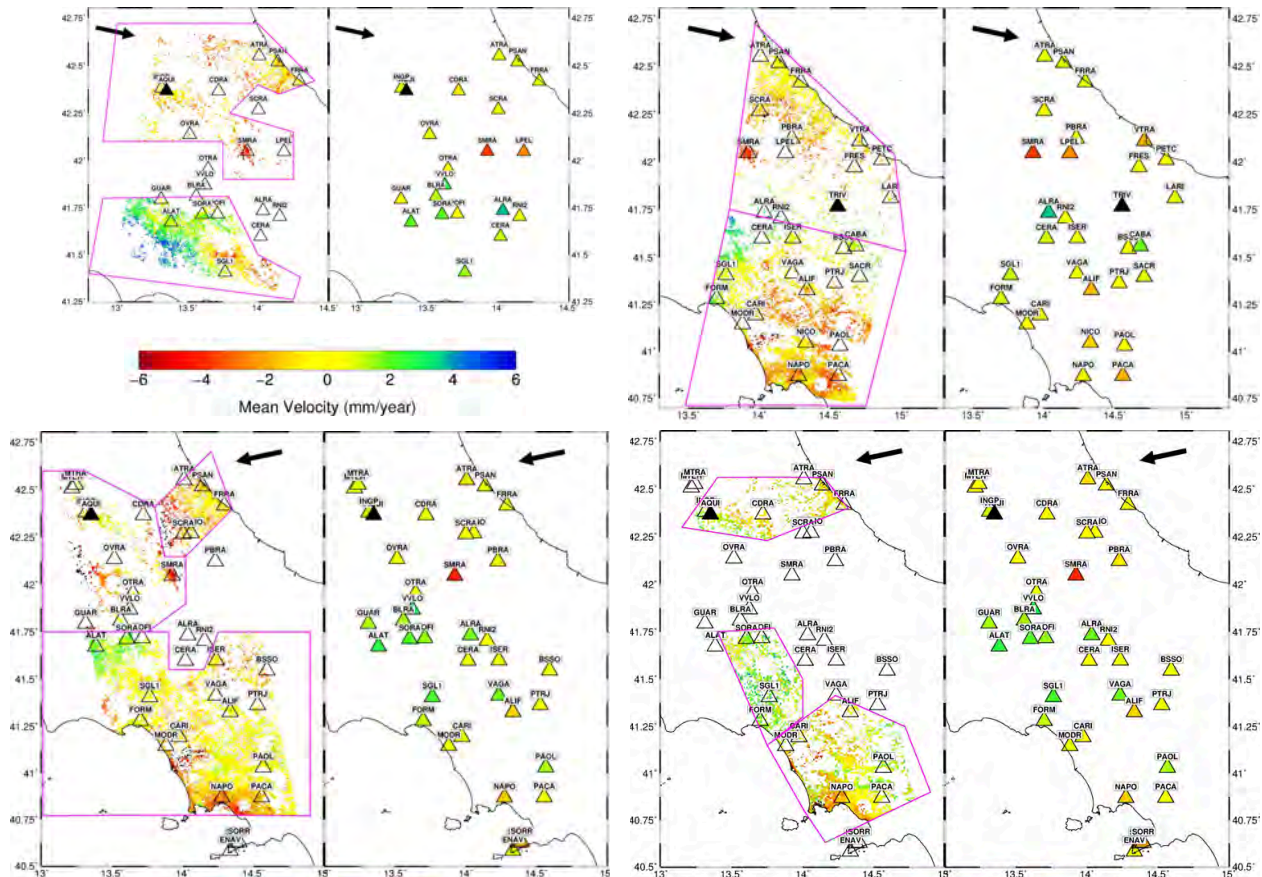


Figure 6. Mean LoS velocities measured from SAR and LoS-projected GPS: ENVISAT desc. track 308 processed with StaMPS (top-left), ENVISAT desc. track 36 processed with StaMPS (top-right), ENVISAT asc. track 129 measured with StaMPS (bottom-left), ERS-1/2 and ENVISAT asc. track 129 measured with ISBAS (bottom-right). Black triangles indicate the reference point or GPS station. The black arrows indicate the ground projection of the SAR LoS (positive from ground to satellite). Magenta polygons enclose the areas within which GPS calibration was performed.

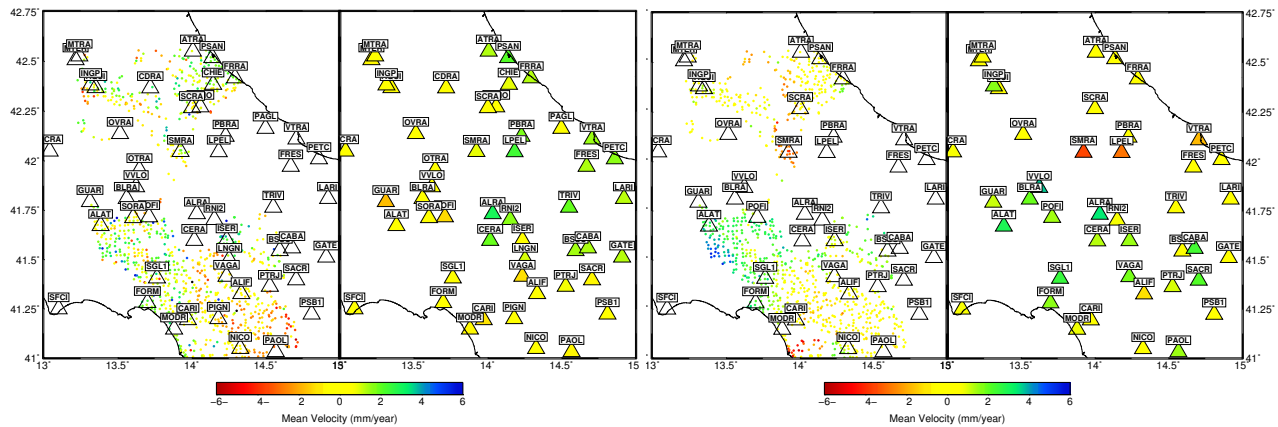


Figure 7. East velocities (left) and Up velocities (right) measured from SAR and LoS-projected GPS

SAR E-W measurements (Fig. 7) are broadly consistent with GPS, although due their limited coverage they cannot confirm or disconfirm the local deformation patterns discussed above. However, within the development area SAR measurements confirm the

slow extension (< 1.5 mm/yr) occurring between the central Apennines and the coast, in agreement with several GPS stations (AQUI-CDRA-PSAN-FRRA transect).

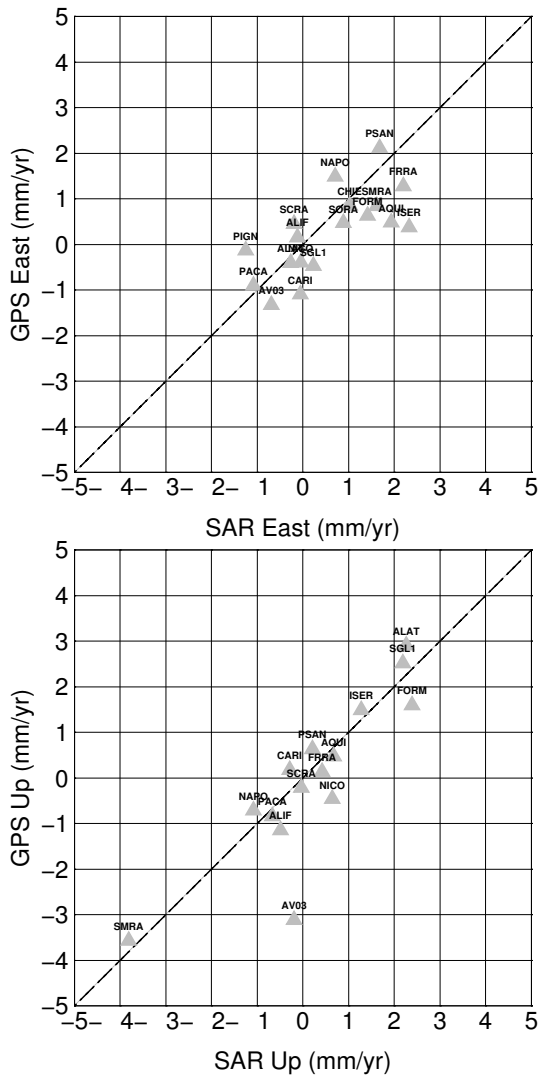


Figure 8 Comparison of SAR and GPS East (top) and Up (bottom) velocity components.

3.2. Earthquake Rates

We present the results of two NeoKinema model runs. For the first (MODEL1), the only geodetic constraints were provided by the GPS measurements. For the second (MODEL2), input was provided by the East and Up components based on SAR measurements (previously calibrated with LoS-projected GPS measurements) and by the North component measured by GPS, interpolated on the same grid.

For MODEL1, the resulting strain and earthquake rates (for events with $M_w > 5.0$) show peaks in the Apennines and in some volcanic areas (Campi Flegrei, Colli Albani). There is an overall agreement between forecasted seismicity and recorded earthquakes (Fig. 9, top), albeit for volcanic areas, where, however, predictions resulting from the geodetic data cannot be considered representative of long-term seismicity.

For the SAR-based model (MODEL2), the resulting strain and earthquake rate maps are more scattered and do not seem to be correlated with past earthquakes (Fig. 9, bottom).

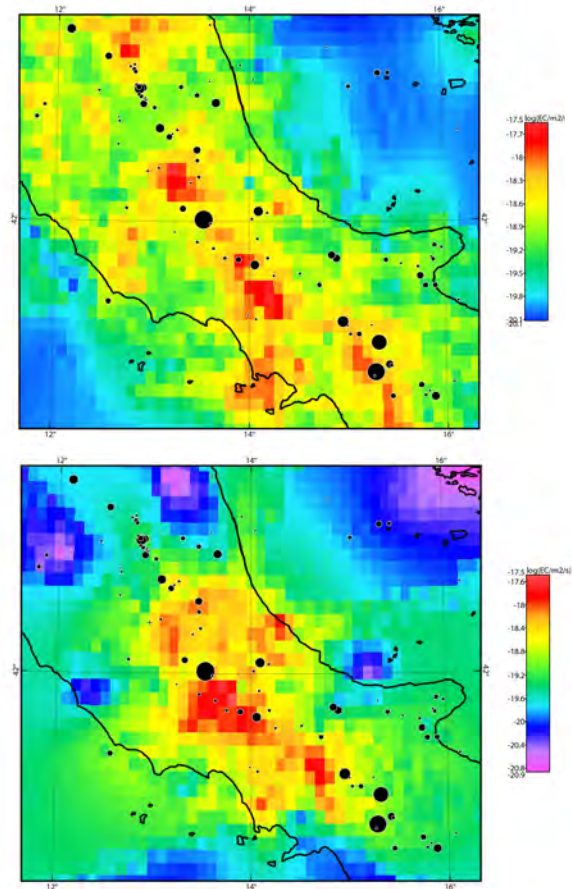


Figure 9 Predicted earthquake rates for GPS-based MODEL1 (top) and SAR-based MODEL2 (bottom). Historical earthquakes (1900-2006) from CPTI11 [16] are shown in black.

3.3. Seismic Hazard

Using the procedure described in section 2.4 we obtained PSHA maps for horizontal peak ground acceleration (PGA) at 10% and 2% probabilities of exceedance in 50 years (or return periods of 500 and 2500 years), for hard ground conditions ($V_s30 > 1000\text{m/s}$). The former are shown in Fig. 10 (top) for earthquake rates based on MODEL1 (GPS data) and in Fig. 10 (bottom) for earthquake rates obtained using MODEL2 (SAR data). In the GPS-based results we can identify 4 areas with the highest values of PGA, all within the Apennines. The SAR-based PSHA model returns a completely different picture of seismic hazard, with the highest value of PGA (10% p.o.e in 50 years) at the intersection of Abruzzi, Latium and Molise, and an area of (saturated) 1g of PGA with 2% of p.o.e in 50 years that almost covers the Abruzzi region.

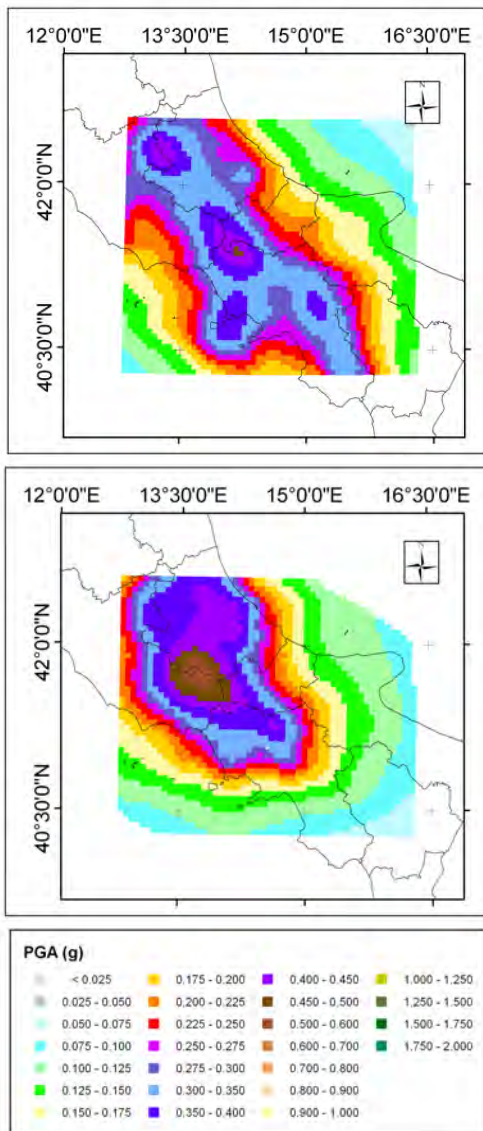


Figure 10 Map of PGA at 10% of probability of exceedance in 50 years, $V_{s30}=1000\text{m/s}$ derived from GPS-based (top) and SAR-based (bottom) earthquake rates.

We validate our results against two data sources: macroseismic intensity histories from the DBMI04 catalogue (<http://emidius.mi.ingv.it/DBMI04/>) and accelerometric recordings from the ITACA 2.0 database (<http://itaca.mi.ingv.it>). Concerning the former, we used the historical record of macroseismic intensities experienced at 9 Italian sites (Fig. 11) to calculate the rates of exceedance from $MI \geq III$. Concerning accelerometric data we selected stations continuously operating for long times and for which a soil classification was given, following the National Seismic Code NTC08 (NTC, 2008). A total of 19 stations were chosen (Fig. 11), 5 of which located on soil A type, and 14 on soil B type.

We test if the number of observed exceedances is consistent with those forecasted by considering

separately the probabilities of observing (1) at least and (2) at most the number of observed events. Outputs from selected sites are shown in Fig. 12. In general, the SAR-based PSHA model tends to return annual frequency of exceedance (AFOE) curves which are higher than the GPS-based model at sites located in the Abruzzi and Lazio regions and viceversa at sites located in the southern Italy. Compared to the accelerometric dataset both geodetic models generally overpredict and never underpredict the observations at the threshold level of 0.001g . In comparison with the macroseismic intensity dataset, the GPS model overpredicts observations only for the Napoli site and underpredicts them at Foggia and Potenza.

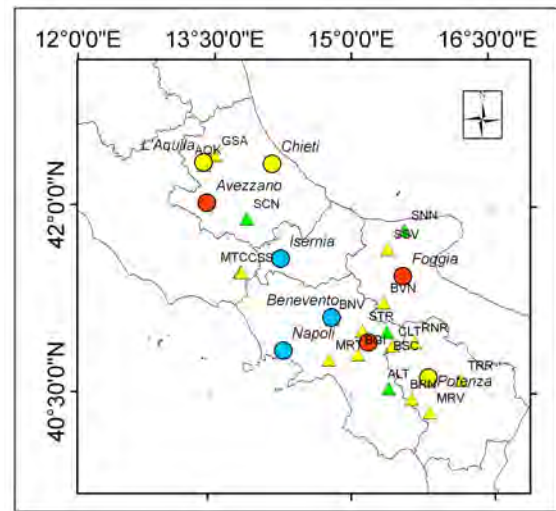


Figure 11 Sites used for validation: accelerometric stations (triangles), selected municipalities with seismic histories in macroseismic intensity (circles). Colours key: green for soil A conditions, yellow for soil B, blue for soil C and red for soil D.

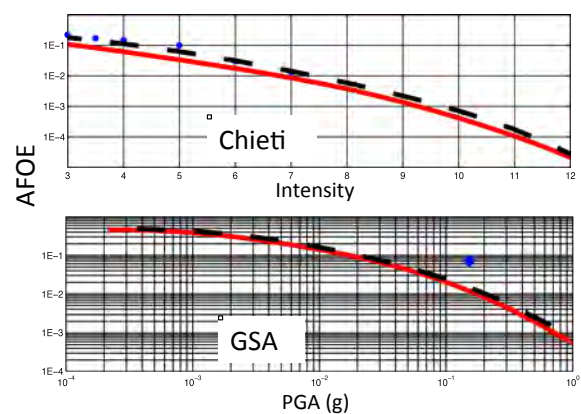


Figure 12 Example of PSHA output validation based on macroseismic intensities (top row) and accelerometric stations (bottom row) for the GPS-based (red curve) and the SAR-based model (dashed black curve). The y-axis indicates the Annual Frequency of Exceedance (AFOE).

4. CONCLUSIONS

GPS and SAR deformation rates of the central Apennines show several gradients of local to regional scale consistent with known seismic sources and regional kinematics. While GPS is essential to capture the long-wavelength patterns (>30 km), SAR has the potential to "fill in the gaps" between GPS measurements and provide a context for these, thus defining more clearly the spatial extent of deformation patterns and the location of transition zones.

Exploitation of the ~20 year long ERS and ENVISAT catalog for seismic hazard applications requires more effort from the measurement point of view, to increase the reliability of the measurements in particular concerning phase unwrapping, and from the modelling point of view, to handle fine spatial scales, measurement noise properties, and coverage gaps.

In our preliminary validation, seismic hazard forecasts driven by geodetic data appear to overestimate ground motions, when compared to macroseismic intensities and accelerometric data. Further validation sites, as well as a more detailed analysis, are required to suggest some explanations for this.

5. REFERENCES

1. Beutler, G., et al. (2002). Bernese GPS Software Version 5.0. In: Dach R., Hugentobler U., Fridez P., Meindl M. (Eds), Astronomical Institute, University of Bern.
2. Altamimi, Z., Collilieux X. & Métivier L. (2011). ITRF2008: An improved solution of the International Terrestrial Reference Frame, *J. Geod.* **85**(8), 457–473.
3. Wdowinski, S., Bock, Y., Zhang, J., Fang, P., Genrich, J. (1997). Southern California Permanent GPS Geodetic Array: Spatial filtering of daily positions for estimating coseismic and postseismic displacements induced by the 1992 Landers earthquake. *J. Geophys. Res.* **102**(B8), 18057–18070.
4. Working Group, DISS, (2010). Database of Individual Seismogenic Sources (DISS), Version 3.1.1: a compilation of potential sources for earthquakes larger than M 5.5 in Italy and surrounding areas. (<http://diss.rm.ingv.it/diss/>).
5. Hooper A. (2008). A multi-temporal InSAR method incorporating both persistent scatterer and small baseline approaches. *Geophys. Res. Lett.*, **35**, L16302.
6. Sowter A., Bateson L., Strange P., Ambrose K. & Syafudin M. (2013). DInSAR estimation of land motion using intermittent coherence with application to the South Derbyshire and Leicestershire coalfields, *Rem. Sens. Lett.*, **4**(10), 979-987.
7. Marinkovic, P. & Larsen Y. (2013). Consequences of long-term ASAR local oscillator frequency decay—an empirical study of 10 years of data, European Space Agency, in *Proc. of the Living Planet Symposium (abstract)*, Edinburgh, U.K.
8. Liu Z. & Bird P. (2008). Kinematic modelling of neotectonics in the Persia-Tibet-Burma orogen, *Geophys. J. Int.*, **172**(2), 779-797
9. Bird P. & Liu Z. (2007). Seismic hazard inferred from tectonics: California, *Seismol. Res. Lett.*, **78**(1), 37-48.
10. Bird, P. & Kagan, Y.Y. (2004) Plate-tectonic analysis of shallow seismicity: Apparent boundary width, beta, corner magnitude, coupled lithosphere thickness, and coupling in seven tectonic settings, *Bull. Seismol. Soc. Am.*, **94**(6), 2380-2399, plus electronic supplement.
11. Cornell C.A., (1968). Engineering seismic risk analysis. *Bulletin of the Seismological Society of America*, **58**(5), 1583-1606.
12. McGuire RK. (2008). Probabilistic seismic hazard analysis: Early history. *Earthquake Engineering & Structural Dynamics*, **37**(3), 329-338.
13. Bindi, D., Pacor, F., Luzi, L., Puglia, R., Massa, M., Ameri, G., Paolucci, R., 2011. Ground motion prediction equations derived from the Italian strong motion database. *Bulletin of Earthquake Engineering* **9**, 1899-1920.
14. Pagani, M., Monelli, D., Weatherill, G., Danciu, L., Crowley, H., Silva, V., Henshaw, P., Butler, L., Nastasi, M., Panzeri, L., Simionato, M., Viganò, D., 2014. OpenQuake Engine: An Open Hazard (and Risk) Software for the Global Earthquake Model, *Seis. Res. Lett.*, **85**, 692-702.
15. D'Agostino, N., R. Giuliani, M. Mattone & L. Bonci, (2001). Active crustal extension in the Central Apennines (Italy) inferred from GPS measurements in the interval 1994–1999. *Geophys. Res. Lett.*, **28**(10), 2121–2124
16. Rovida, A., Camassi R., Gasperini P. & Stucchi M. (eds.), (2011). CPTI11, the 2011 version of the Parametric Catalogue of Italian Earthquakes. Milano, Bologna, <http://emidius.mi.ingv.it/CPTI>.